ACES Asian Chemical Editorial Society

DOI: 10.1002/asia.202000336

CHEMISTRY AN ASIAN JOURNAL Full Paper

Special Collection

Au Nanoparticles Modified with Pt, Ru and SnO_2 as Electrocatalysts for Ethanol Oxidation Reaction in Acids

Kumar Siddharth[+],[a] Zelong Xing[+],[a] Fei Xiao[+],[a] Shangqian Zhu,[a] Lili Zhang,[a, b] Feng Pan,[c] and Minhua Shao*[a]

Abstract: The anodic reaction in direct ethanol fuel cells (DEFCs), ethanol oxidation reaction (EOR) faces challenges, such as incomplete electrooxidation of ethanol and high cost of the most efficient electrocatalyst, Pt in acidic media at low temperature. In this study, core-shell electrocatalysts with an Au core and Pt-based shell (Au@Pt) are developed. The Au core size and Pt shell thickness play an important role in the EOR activity. The Au size of 2.8 nm and one layer of Pt provide the most optimized performance, having 6 times higher peak current density in contrast to commercial Pt/C. SnO_2 as a support also enhances the EOR activity of Au@Pt by 1.73 times. Further modifying the Pt shell with Ru atoms achieve the highest EOR current density that is 15 and 2.5 times of Pt/C and Au@Pt. Our results suggest the importance of surface modification in rational design of advanced electrocatalysts.

Introduction

Direct ethanol fuel cells (DEFCs) are crucial with respect to energy and environment as ethanol possess higher energy density (8.0 kWh/kg, 6.34 kWh/L) compared to hydrogen and other alcohols such as methanol, ethylene glycol and glycerol; can be sustainably produced from biomass and it possesses low toxicity as well as favourable handling infrastructure.[1] The anodic ethanol oxidation reaction (EOR) requires highly active electrocatalysts for complete conversion of ethanol to CO_2 by breaking the C–C bond.[2]

Pt has been recognized as the most effective electrocatalyst for EOR. However, pure Pt in the ethanol oxidation process is susceptible to self-poisoning and exhibits poor selectivity.[3] The activity and selectivity of the Pt catalysts can be enhanced by adding different metals to form a binary or ternary catalyst is a common strategy. Elements such as Ru,[4] Rh,[5] Ni,[6] Bi,[7] Au,[8] Pd,[1e,5a,7c,8] Cu[9] and Sn[10] have been widely used to increase the electrochemical performance, out of which Ru and Sn provided more efficient designs. In one study, it was found that Pt_{46}-$(SnO_2)_{54}$ non-alloyed core–shell particles illustrated better C–C bond cleavage capability than intermetallic Pt/Sn.[10e] Some elements like Ru adsorb oxygenated species such as OH_{ads} easily, which leads to easier oxidation of CO intermediates to CO_2, increasing the activity manifold while some other elements can assist in C–C bond cleavage. In one interesting study, ternary catalyst Pt–Rh-SnO_2/C electrocatalyst achieved very high electrocatalytic performance in terms of both selectivity and activity. Through the combination of experimental analysis and density functional theory (DFT) calculations, it was illustrated that interactions of three constituents with specific properties could be the reason for its extraordinary electrocatalytic performance.[11] EOR performance is also affected by the particle size of the catalyst[12] as well as ligand and strain effects.[13] Nonetheless, more studies are required to design efficient and cost-effective Pt-based electrocatalysts for EOR.

Core-shell structures are one of the most effective ways to reduce the loading of noble metal while, at the same time has the ability to increase catalyst efficiency by virtue of strain effect.[14] Surface modification is another technique which could help in designing better electrocatalysts by making use of the bifunctional mechanism.[15] In a very intriguing work, electrocatalysts were synthesized through Pt monolayer deposition on different substrates (bulk (111) single crystals). A correlation between strain effect in the Pt monolayer and its electrochemical performance for EOR was established. It was observed that a wide mismatch of lattice (~4% tensile strain) and electronic synergy (ligand effect) between the Pt shell and Au core could upshift the d-band center of Pt which resulted in stronger binding of adsorbates leading to an increase in EOR activity.[16] Taking this work forward, in this study, binary catalysts based on the core-shell structure with the core being Au nanoparticles and Pt as shell were synthesized by the classic process with two steps. Firstly, a Cu monolayer is underpotentially deposited (UPD) on Au nanoparticle surface. Subsequently, replacement of Cu with Pt is carried out via the galvanic redox procedure in a Pt(II)-containing solution.[17] The

[a] *K. Siddharth,[+] Z. Xing,[+] F. Xiao,[+] Dr. S. Zhu, Prof. L. Zhang, Prof. M. Shao*
Department of Chemical and Biological Engineering
The Hong Kong University of Science and Technology
Clear Water Bay, Kowloon (Hong Kong)
E-mail: kemshao@ust.hk

[b] *Prof. L. Zhang*
Jiangsu Key Laboratory for Chemistry of Low-Dimension Materials
Huaiyin Normal University
Huaian 223300, Jiangsu (China)

[c] *Prof. F. Pan*
School of Advanced Materials
Peking University
Shenzhen Graduate School
Shenzhen (China)

[+] *These authors contributed equally to this paper.*

Supporting information for this article is available on the WWW under https://doi.org/10.1002/asia.202000336

Special Collection *This manuscript is part of a special collection on Interface Chemistry for Electrochemical Energy Applications.*

core size and shell thickness effects on ethanol oxidation were examined and it was found that Au core size of 2.8 nm gave the best performance while as the Pt shell layer increased, Au substrate effect gradually diminished. The most optimized Au@Pt core-shell electrocatalyst illustrated forward peak current density six times the commercial Pt/C. The effect of SnO_2 and further surface modification of the Pt shell with Ru adatoms were also explored on the core-shell catalysts.

Results and Discussions

TEM images of five Au NPs on carbon black support with contrasting sizes together are shown in Figure 1 and the respective particle size distribution histograms are illustrated in Figure S1. The shape of all the five samples are roughly spherical and are uniformly dispersed on the support i.e. carbon. The sizes of 200 particles chosen from their TEM images randomly are averaged to draw the mean size of the nanoparticles, and the corresponding sizes are following: (a, b, c) 1.9 $\pm$0.3 nm; (d, e, f) 2.8$\pm$0.4 nm; (g, h, i) 3.6 $\pm$0.3 nm; (j, k, l) 4.8 $\pm$0.4 nm and (m, n, o) 5.6$\pm$1.1 nm.

Figure 2a illustrates a typical CV of 2.8 nm Au NPs with a range of 0.05 V-1.6 V (vs RHE) in 0.1 M $HClO_4$ solution saturated with Ar. The Cu UPD result of the cleaned Au NPs in a 50 mM $CuSO_4$ + 50 mM H_2SO_4 solution saturated with Ar at 5 mV s^{-1} scan rate is elucidated by the black line in Figure 2b. Two distinct current peaks were seen at 0.58 V and 0.6 V, on the cathodic and anodic scans, respectively. The 0.58 V peak was assigned to Cu UPD on Au surface, whereas the peak at 0.6 V corresponds to stripping of Cu, consistent with the literature.[19] The electrochemical surface area (ECA) of Au NPs was calculated based on the Cu monolayer stripping charge. The ECA of Au NPs in Figure 2 was estimated to be 0.18 cm^2, considering 420 $\mu C\,cm^{-2}$ for a complete monolayer coverage of Cu.[20] Immersion of the Cu monolayer shrouded Au NPs was carried out in a 1.0 mM K_2PtCl_4 + 50 mM H_2SO_4 solution saturated with Ar to displace Cu with Pt to form an alike core-shell structure (Au@Pt). The CV of Au@Pt is also shown by the red line in Figure 2a. A pair of distinct peaks originating from the H adsorption/desorption was seen in 0.05-0.32 V potential range. These peaks were identical to that of Pt/C, elucidating the successful deposition of a Pt layer on Au NPs.[21]

After the deposition of Pt atoms on Au NPs surfaces, one distinct pair of wide peaks related with Cu UPD on Pt was detected, the peak at 0.60 corresponded to deposition and the peak at 0.57 V was assigned to stripping. This observation demonstrated the Pt layer presence. This pair of broad peaks became more distinct as the Pt layers grew on the Au core, as illustrated in Figure 2b. However, the Cu UPD curves of the Au@Pt and Pt/C are not similar. This result highlights that current contribution comes from both Au and Pt atoms in the Au@Pt Cu UPD curve. The surface area obtained via the charge of Cu UPD (from both Pt and Au atoms) is 0.24 cm^2. This value is larger than the Pt area obtained via hydrogen adsorption (0.17 cm^2), and Au area calculated from Cu UPD (0.20 cm^2). The Pt coverage is found to be 0.7-0.8 on the basis of these values. The Au@Pt structure containing Pt clusters on the surfaces of Au is depicted in the inset of Figure 2a.

The characteristics of Au@Pt NPs are further revealed by the STEM results, which are shown in Figure 3. According to the SETM results, it can be observed that the identical core-shell NPs are dispersed on the support (carbon), with negligible agglomeration. Besides, it is confirmed by the EDX 2D mapping of an individual Au@Pt NP that a Pt overlayer exists. However, due to the resolution limitation, Figure 3 can not tell whether the coverage of the Pt layer.

Figure 4 shows the linear sweep voltammetric scans for Pt and Au@Pt with five distinct core sizes in 0.1 M $HClO_4$ and 0.2 M ethanol with a scan rate of 50 mV s^{-1}. The EOR activities of Au@Pt with distinct Au particle sizes (1.9, 2.8, 3.6, 4.8, and 5.6 nm) are analyzed in Figure 4 and Table 1. The corresponding ECAs calculated from Cu UPD were used to normalize the currents. The linear sweep voltammograms, EOR onset potentials and current peak potentials for the five samples exhibited similar characteristics, at the same time the peak current density reach maximum for Au particle size 2.8 nm. The total mass activity (Pt + Au) of the Au@Pt with the best specific activity at the maximum current was 983.2 mA mg^{-1}, which is 5.83 times of that Pt/C (168.6 mA mg^{-1}). It was seen that the specific activity of Au@Pt of all sizes were at least three times greater in comparison to pure Pt/C with respect to peak current density, pinpointing the significance of Au and Pt synergistic effect. Au@Pt with a size of 2.8 nm illustrated the maximum increase in EOR activity with six times more peak current density compared to Pt/C. Onset potential was negatively shifted by ~400 mV as well for all the core-shell electrocatalysts compared to Pt/C as seen in Table 1, indicating the positive effect of Au core in increasing the EOR activity and lowering the overpotential. The significant increase in activity can be assigned to the effects of strain resulting from the substrate materials according to previous literature.[16] A large mismatch of lattice (tensile strain of about 4%) between the Au substrate and the Pt layer causes an upshift of the d-band centre of the Pt shell. The adsorbates tend to bind more strongly due to the higher-lying d-band centre, leading to an increase in EOR activity for the Pt shell in an acidic medium.[16] Strasser and co-workers compared the C–C bond splitting ability of Pt overlayers on Au NPs with Pt and found that the former was more efficient to break the C–C bond.[13] The results in this study are consistent with the literature that the Au core can enhance the activity of Pt overlayers by assisting the C–C bond breaking.

Shell thickness effect was also investigated by depositing 1–5 layers of Pt on the Au core of the most optimized size 2.8 nm

Table 1. The onset potential and peak current density (*j*) of EOR on different catalysts

Catalyts	Onset potential [V]	*j* [mA cm^{-2}]
Pt/C	0.76	0.28
Au@Pt/C (1.9 nm)	0.30	0.93
Au@Pt/C (2.8 nm)	0.33	1.68
Au@Pt/C (3.6 nm)	0.35	1.50
Au@Pt/C (4.8 nm)	0.30	1.11
Au@Pt/C (5.6 nm)	0.35	0.91

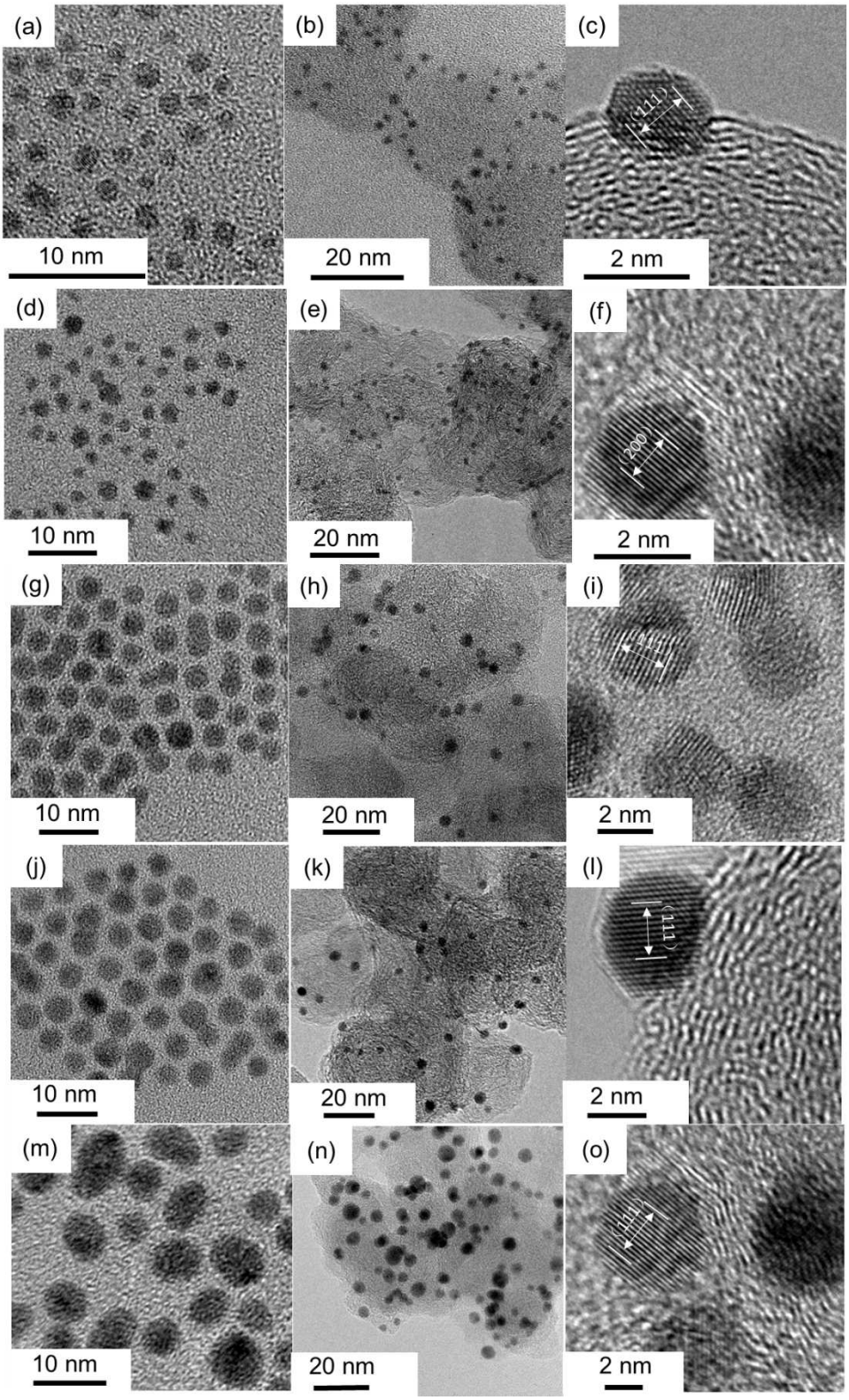

Figure 1. TEM images of Au NPs with contrasting particle sizes (a, b, c) 1.9 ± 0.3 nm, (d, e, f) 2.8 ± 0.4 nm, (g, h, i) 3.6 ± 0.3 nm, (j, k, l) 4.8 ± 0.4 nm, (m, n, o) 5.6 ± 1.1 nm

through a layer by layer approach utilizing the Cu UPD method.[20] The CV curves of Au@Pt with various numbers of Pt layers in 0.1 M $HClO_4$ solution saturated with Ar are depicted in Figure S2a. With an increase in the layers of Pt, the hydrogen adsorption/desorption current density enhances progressively as expected by virtue of the increase in surface area. Similar

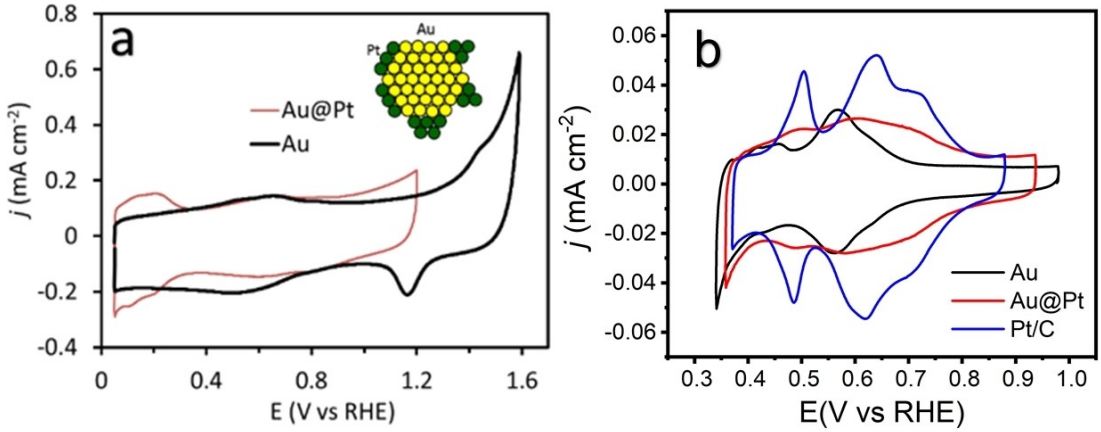

Figure 2. CVs of Au NPs (black line), Au@Pt (red line) and Pt/C (blue line) electrodes in (a) 0.1 M $HClO_4$ solution, (b) 0.05 M H_2SO_4 + 0.05 M $CuSO_4$ solution saturated with Ar; the Au@Pt structure model is demonstrated in the inset of Figure 2a. (Au particle size 2.8 nm)

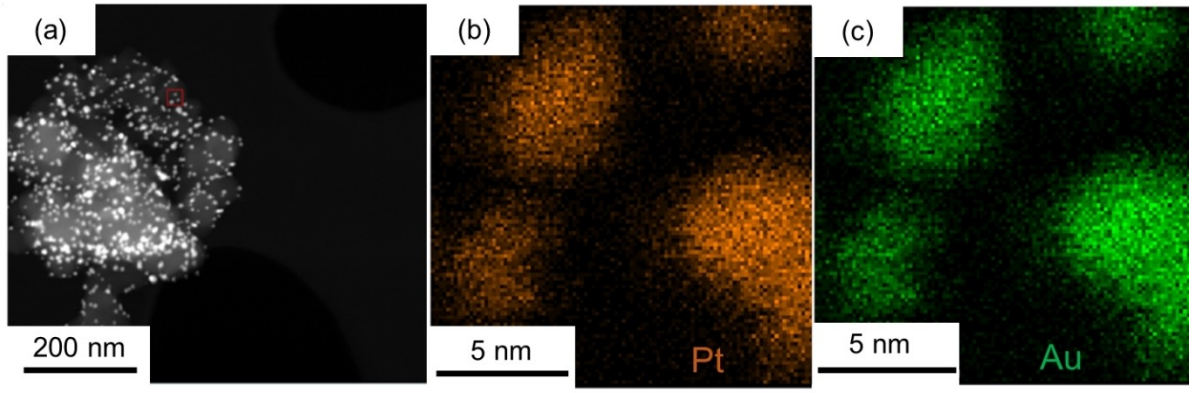

Figure 3. (a) HAADF-STEM image and EDX mapping results for platinum (b) and gold (c) for the area of (a) in the red inset square.

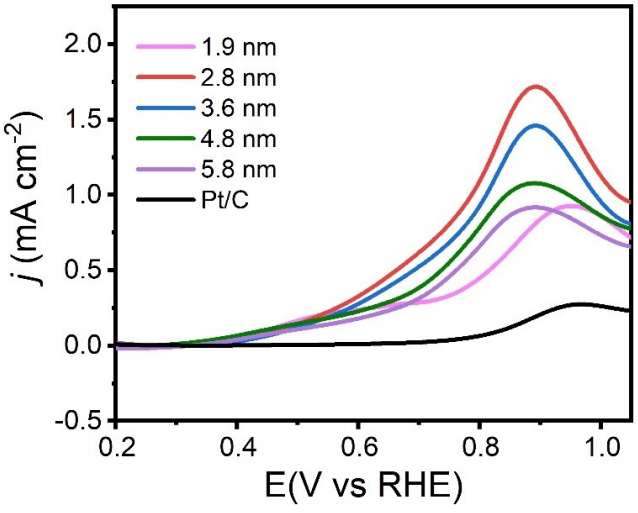

Figure 4. Linear sweep voltammograms of ethanol electrooxidation in 0.1 M $HClO_4$ + 0.2 M ethanol solution saturated with Ar at a scan rate of 50 mV s^{-1} for Au@Pt with distinct Au particle sizes. Respective ECAs were used to normalize the currents.

results were observed by Shao et al.[20] and Han et al..[22] Figure S2b illustrates the Cu UPD curves of five different kinds of Pt monolayer-modified Au nanoparticles in a 0.05 M H_2SO_4 + 0.05 M $CuSO_4$ solution at 5 mV s^{-1} scan rate which indicates a similar current density increase in terms of Cu deposition/stripping. The features of the Cu UPD curves for Au@Pt with two or more layers of Pt are identical with that of Pt/C indicating higher coverages of Pt atoms than that with only one layer.

Figure 5 elucidates anodic voltammetric scans for Pt/C and five different kinds of Pt layer-modified Au NPs in 0.1 M $HClO_4$ + 0.2 M ethanol with a scan rate of 50 mV s^{-1}. The respective ECAs calculated from Cu UPD were used to normalize the currents. The peak current density of each curve falls as the number of Pt layers increases from one to five. As stated earlier, the upshift of the d-band centre of the Pt might be caused by the structure of Au@Pt, resulting in a stronger OH and ethanol adsorption. As a result of these ligand and strain effects, the electrocatalytic activity of Pt is enhanced.[16] Since this Au substrate effect is reduced as the Pt layer increases, the activity of Au@Pt catalysts for EOR decreases. However, it is difficult to estimate at what thickness of the Pt shell the substrate effects were completely absent. Our previous study on Pt shell on

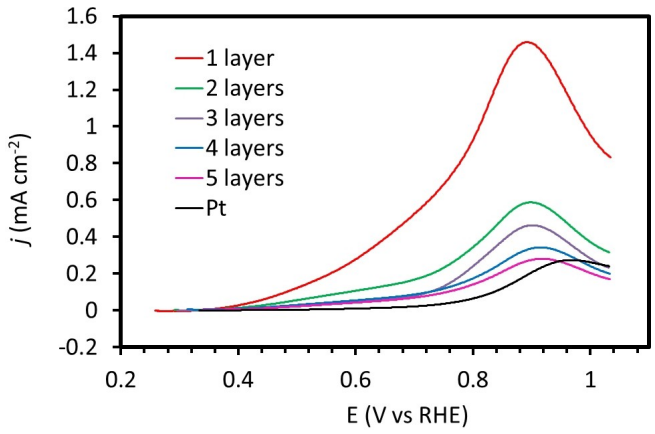

Figure 5. Linear sweep voltammograms of ethanol electrooxidation in 0.1 M $HClO_4$ + 0.2 M ethanol solution saturated with Ar at 50 mV s^{-1} scan rate for Au (2.8 nm) substrate with 1–5 Pt layers and Pt/C.

Pt–Ni alloy nanoparticles suggested that the substrate effect could only extend up to 3 Pt layers.[23] We expect the similar trend to occur in the Au@Pt system, which was confirmed by the fact the peak current densities of the samples with 4 and 5 Pt layers approached to that of pure Pt. It should be emphasized that the reduction of peak current density between the one and two layers is much more obvious than for the others, implying a dramatic decrease in the catalytic activity of Pt atoms. Furthermore, the peak current density of the sample with five Pt layers is almost the same as that of Pt implying that the effect from the Au core almost diminished.

For further enhancement of the EOR activity of Au@Pt, two strategies were adopted: addition of SnO_2 by the process mentioned in section 2.3 and surface modification by Ru atoms conducted by a simple dipping process. Figure 6a compares the LSVs for Pt/C, Au@Pt, Au@Pt/SnO_2, Au@Pt–Ru and Au@Pt–Ru/SnO_2 in Ar-saturated 0.1 M $HClO_4$ + 0.2 M ethanol with 50 mV s^{-1} scan rate. The respective ECAs calculated from Cu UPD were used to normalize the currents. When the Au nanoparticles were supported on SnO_2, the EOR activity could be increased by 1.73 times compared to Au@Pt as seen in Figure 6a with Au@Pt/SnO_2 illustrating a forward peak current density of 2.90 mA cm^{-2}. The corresponding CO stripping curves of Au@Pt/SnO_2 and Au@Pt are compared in Figure 6b. The latter showed a clear CO stripping peak at 0.84 V, which is 60 mV lower than that of Pt/C. For the Au@Pt/SnO_2 sample, the main stripping peak was 40 mV lower than that of Au@Pt. More interestingly, the CO oxidation current appeared as low as 0.1 V forming a pre-peak at 0.6 V. Both features suggest that poisonous CO species are removed at a lower potential for Au@Pt/SnO_2 and highlight the key role of SnO_2 in improving the EOR activity by providing OH species at very low potentials.

The surface modification effect by Ru atoms are even more obvious. To validate the successful deposition of Ru, Figure S3a compares the CVs of Au@Pt–Ru and Au@Pt in 0.1 M $HClO_4$ saturated with Ar at a scan rate of 50 mV s^{-1}. Two well-defined peaks by virtue of hydrogen adsorption and desorption on the catalysts surface were seen between 0.02-0.38 V in each CV curve. When Ru was deposited on the Au@Pt/C surface, the charges in the realm of hydrogen adsorption and desorption was smaller, which could be explained by the reduction of available Pt sites due to Ru deposition. Similar attenuation was observed in case of Au@Pt/SnO_2 and Au@Pt–Ru/SnO_2 as illustrated in Figure S3b. Au@Pt–Ru displays a peak current density of 3.82 mA cm^{-2} during EOR (Figure 6a), which is significantly higher than those of Au@Pt and Au@Pt/SnO_2. With the presence of Ru, water dissociates actively to form hydroxides at lower potentials compared to that on Pt.[11] Therefore, the poisoning intermediates, such as CO and CH_x, can be oxidized and leads to relatively higher EOR performance. The CO stripping curves of Au@Pt–Ru and Au@/Pt are also analyzed in Figure 6b. The CO oxidation started as low as 0.3 V and peaked at 0.7 V, which was 140 mV lower than that of Au@Pt. When the same Ru surface modification strategy was applied to Au@Pt/SnO_2, the best EOR performance was observed with a peak current density of 4.25 mA cm^{-2}, which is 15 and 2.5 times of that of Pt/C and Au@Pt, respectively. Compared with Au@Pt–Ru, the EOR onset potential on Au@Pt–Ru/SnO_2 was similar but the potential of the peak current was shifted by

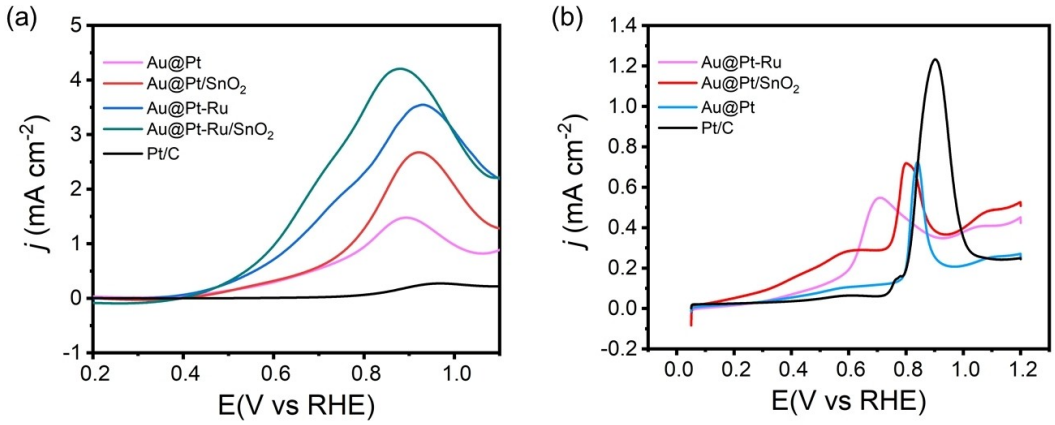

Figure 6. (a) Linear sweep voltammograms of Pt/C, Au@Pt–Ru/SnO_2, Au@Pt–Ru, Au@Pt/SnO_2 and Au@Pt in 0.1 M $HClO_4$ + 0.2 M ethanol solution saturated with Ar at 50 mV s^{-1} scan rate. (b) CO stripping curves are measured in 0.1 M $HClO_4$ solution saturated with Ar at 50 mV s^{-1} scan rate for Pt/C, Au@Pt, Au@Pt–Ru, and Au@Pt and Au@Pt/SnO_2.

40 mV negatively. In accordance with the Langmuir-Hinshelwood mechanism, more oxophilic materials such as Ru and SnO_2 can generate adsorbed OH that is necessary for removal of poisonous CO_{ad} at lower potentials than Pt, thus leaving more active sites of Pt for ethanol oxidation.[24]

Conclusion

In this study, core-shell electrocatalysts based on Au core and Pt shell were developed. Five groups of Au NPs were synthesized with size ranging from 1.9 to 5.6 nm. When the surfaces of Au nanoparticles were deposited a layer of Pt atoms forming an identical core-shell structure (Au@Pt), all the Au samples exhibited high activities for EOR, elucidated by at least 3 times increase in current density compared to Pt/C as well as negative shifts in onset potential. The Au core size effect on EOR activity was analysed and it was found that 2.8 nm provided the most optimized performance, having 6 times larger peak current density in contrast to commercial Pt/C. Moreover, Pt shell effect was demonstrated by finding out that the Au substrate effect decreased as the Pt layer increased, leading to the reduction of EOR activity. Metal oxide support like SnO_2 also can play a significant role in enhancing EOR activity as its addition increased the activity of Au@Pt by 1.73 times. Further modifying the Pt shell with Ru atoms could greatly improve the overall EOR performance. The highest EOR current density was observed on Au@Pt–Ru/SnO_2 that was 15 and 2.5 times of Pt/C and Au@Pt, respectively. Our results demonstrate the significance of surface modification and bifunctional approaches in rational design of advanced electrocatalysts.

Experimental section

Preparation of Au NPs

Carbon-supported gold nanoparticles (Au NPs) were synthesized following a previous study.[18] Briefly, a well stirred solution of 10 mL toluene containing 0.15 g tetraoctylammonium bromide was put into deionized water (5 mL) consisting of 0.031 g $HAuCl_4{\cdot}3H_2O$. Then, addition of 0.046 g of dodecanethiol was carried out. It was followed by isolation of the organic phase and vigorous stirring of the corresponding solution was carried out at room temperature for 10 min. 5 mL of deionized water containing 0.038 g of $NaBH_4$ was further added for periods of 10 s, 2 min or 10 min, leading to generation of different Au particle sizes. The dark organic phase was further stirred for at least another 3 h at room temperature. After the collection of organic phase, rotary evaporator was used to remove the solvent. The product was obtained via centrifugation for 3 times in 10 mL of ethanol and 20 mL of acetone. Au nanoparticles of measured amount were put into a carbon black suspension, followed by 30 min sonication, and finally stirring it overnight. The nanoparticles supported on carbon were then collected and Ar atmosphere was used to dry them. Subsequently, they were treated in a tube furnace with the temperature and atmosphere pressure being controlled. A regular thermal treatment protocol was followed in which the sample was heated at 280 °C and under 8% H_2/Ar for another 30 minutes.

Preparation of Au@Pt Electrocatalysts

A typical three-electrode cell was used to synthesize core-shell electrocatalysts at room temperature. The reference and counter electrodes used were Ag/AgCl and Pt wire, respectively. A catalyst-covered glassy carbon with 0.196 cm^2 area was utilized as the working electrode. The catalyst ink was prepared by ultrasonication of the mixture of 5 mg of the corresponding catalytic powder, 1 mL of 2-propanol and 2 μL of 5% Nafion in 4 mL of water for 15 min. 10 uL of the catalyst was deposited on glassy carbon electrode surface and infrared lamp was used for drying to get a thin film. Au@Pt electrocatalyst was prepared by a Cu monolayer displaced by galvanic procedure, deposited over the as-synthesized Au/C surface. The activation of Au/C electrode was carried out between 0.05 and 1.6 V for 20 cycles in 0.1 M $HClO_4$ solution at 50 $mV\,s^{-1}$ scan rate before conducting the Cu UPD and the corresponding cyclic voltammogram (CV) curves were recorded. Reversible hydrogen electrode (RHE) was used as reference for all the potentials. The potential for Cu UPD ranged between 0.33 V to 0.75 V at a scan rate of 5 $mV\,s^{-1}$ in a 50 mL solution of 50 mM H_2SO_4 + 50 mM $CuSO_4$. The Au/C electrode, shrouded with a Cu monolayer was then followed by rapid rinsing with water and put in a solution of 1.0 mM K_2PtCl_4 + 50 mM H_2SO_4 for 1 min to displace the Cu with Pt. The as-prepared Au@Pt electrode was obtained and multiple washing with deionized water was carried out.

Preparation of Au@Pt-SnO_2 Electrocatalysts

Initially, SnO_2 colloids were synthesized. Typically, 33.3 mg of $SnCl_2$ was dissolved in 10 mL of ethylene glycol with 2 mL deionized water. The mixture was heated up to 190 °C within 25 min from room temperature and refluxed for 1 hr. It was ready to use after cooling. The resulting solution had a light yellow colour with slightly decreased volume due to the loss of water content. After that, it was mixed with as-synthesized Au NPs suspended in toluene followed by sonication. The product Au-SnO_2 was collected by centrifugation followed by similar procedure mentioned in section 2.2 to obtain the Au@Pt-SnO_2 electrocatalysts.

To modify the Au@Pt and Au@Pt-SnO_2 surfaces with Ru, the electrode containing Au@Pt and Au@Pt-SnO_2 electrocatalyst ink was dipped into 1 mM $RuCl_3$ solution for 1 min, and then multiple washing with deionized water was carried out to obtain the Au@Pt-Ru/SnO_2 electrocatalyst.

Physical Characterizations

In this study, Tecnai F30 electron microscope (FEI; Netherlands) was used to perform the energy dispersive X-ray (EDX) and scanning transmission electron microscopy (STEM) characterizations. TEM was conducted on 2010F machine. TEM, STEM and high-resolution TEM (HRTEM) with a high-angle annular dark-field (HAADF-STEM) studies were conducted by putting a drop of sample hydrosol on a carbon coated copper grid.

Electrochemical Characterizations

CVs of the electrocatalysts were then recorded between 0.05 and 1.2 V for one cycle in 0.1 M $HClO_4$ solution at 50 $mV\,s^{-1}$ scan rate. All the electrolyte solutions in the cell were first purged with argon before the electrochemical measurements for about 30 min. Voltammetric measurements of EOR were carried out in a 0.1 M $HClO_4$ + 0.2 M EtOH solution in the potential range between 0.05 and 1.2 V at 50 $mV\,s^{-1}$ scan rate. For comparison, a commercial Pt/C catalyst (TKK, TEC10E50E, 2.5 nm) was chosen. Before ethanol

oxidation, Pt/C catalysts were activated by potential cycling between 0.05 and 1.2 V at 50 mV s^{-1} scan rate for 10 cycles.

Acknowledgement

This work is supported by a startup fund from the Hong Kong University of Science and Technology.

Conflict of Interest

The authors declare no conflict of interest.

Keywords: Core-shell electrocatalyst · Direct ethanol fuel cells · Ethanol oxidation reaction · Platinum Alloy · Underpotential deposition

[1] a) B. Cermenek, J. Ranninger, V. Hacker, in *Ethanol*, Elsevier, **2019**, pp. 383–405; b) J. Bai, D. Liu, J. Yang, Y. Chen, *ChemSusChem* **2019**, *12*, 2117–2132; c) M. Kamarudin, S. K. Kamarudin, M. Masdar, W. R. W. Daud, *Int. J. Hydrogen Energy* **2013**, *38*, 9438–9453; d) E. Antolini, *J. Power Sources* **2007**, *170*, 1–12; e) X. Yang, Q. Yang, J. Xu, C.-S. Lee, *J. Mater. Chem.* **2012**, *22*, 8057–8062; f) F.-M. Li, X.-Q. Gao, S.-N. Li, Y. Chen, J.-M. Lee, *NPG Asia Mater.* **2015**, *7*, e219-e219; g) P. Wu, Y. Huang, L. Kang, M. Wu, Y. Wang, *Sci. Rep.* **2015**, *5*, 14173; h) J. Guo, R. Chen, F.-C. Zhu, S.-G. Sun, H. M. Villullas, *Appl. Catal. B* **2018**, *224*, 602–611.

[2] a) T. Almeida, Y. Yu, A. De Andrade, H. Abruna, *Electrochim. Acta* **2019**, *295*, 751–758; b) S. Alayoglu, A. U. Nilekar, M. Mavrikakis, B. Eichhorn, *Nat. Mater.* **2008**, *7*, 333–338; c) L. Chen, H. Guo, T. Fujita, A. Hirata, W. Zhang, A. Inoue, M. Chen, *Adv. Funct. Mater.* **2011**, *21*, 4364–4370.

[3] R. Kavanagh, X. M. Cao, W. F. Lin, C. Hardacre, P. Hu, *Angew. Chem. Int. Ed.* **2012**, *51*, 1572–1575; *Angew. Chem.* **2012**, *124*, 1604–1607.

[4] a) G. Camara, R. De Lima, T. Iwasita, *Electrochem. Commun.* **2004**, *6*, 812–815; b) L. Colmenares, H. Wang, Z. Jusys, L. Jiang, S. Yan, G. Sun, R. Behm, *Electrochim. Acta* **2006**, *52*, 221–233; c) A. O. Neto, M. J. d. Giz, J. Perez, E. A. Ticianelli, E. R. Gonzalez, *J. Electrochem. Soc.* **2002**, *149*, A272-A279; d) H. Wang, Z. Jusys, R. Behm, *J. Power Sources* **2006**, *154*, 351–359; e) Q. Wang, G. Sun, L. Jiang, Q. Xin, S. Sun, Y. Jiang, S. Chen, Z. Jusys, R. Behm, *Phys. Chem. Chem. Phys.* **2007**, *9*, 2686–2696.

[5] a) W. Zhu, J. Ke, S.-B. Wang, J. Ren, H.-H. Wang, Z.-Y. Zhou, R. Si, Y.-W. Zhang, C.-H. Yan, *ACS Catal.* **2015**, *5*, 1995–2008; b) R. G. Freitas, E. C. Pereira, P. A. Christensen, *Electrochem. Commun.* **2011**, *13*, 1147–1150.

[6] a) T. Almeida, A. Van Wassen, R. Van Dover, A. De Andrade, H. Abruña, *J. Power Sources* **2015**, *284*, 623–630; b) A. Dutta, J. Ouyang, *ACS Catal.* **2015**, *5*, 1371–1380.

[7] a) M. C. Figueiredo, A. Santasalo-Aarnio, F. J. Vidal-Iglesias, J. Solla-Gullón, J. M. Feliu, K. Kontturi, T. Kallio, *Appl. Catal. B* **2013**, *140*, 378–385; b) M. C. Figueiredo, R. M. Arán-Ais, J. M. Feliu, K. Kontturi, T. Kallio, *J. Catal.* **2014**, *312*, 78–86; c) Y. Huang, J. Cai, M. Liu, Y. Guo, *Electrochim. Acta* **2012**, *83*, 1–6; d) F. Matsumoto, *Electrochemistry* **2012**, *80*, 132–138; e) M. M. Tusi, N. S. Polanco, S. G. da Silva, E. V. Spinacé, A. O. Neto, *Electrochem. Commun.* **2011**, *13*, 143–146.

[8] a) J. Datta, A. Dutta, S. Mukherjee, *J. Phys. Chem. C* **2011**, *115*, 15324–15334; Song, L.-P. Mei, A.-J. Wang, K.-M. Fang, J.-J. Feng, *Int. J. Hydrogen Energy* **2016**, *41*, 1645–1653; b) Y. Peng, L. Li, R. Tao, L. Tan, M. Qiu, L. Guo, *Nano Res.* **2018**, *11*, 3222–3232; c) L. Tan, L. Li, Y. Peng, L. Guo, *Nanotechnology* **2015**, *26*, 505401.

[9] F. Saleem, Z. Zhang, B. Xu, X. Xu, P. He, X. Wang, *J. Am. Chem. Soc.* **2013**, *135*, 18304–18307.

[10] a) W. Du, K. E. Mackenzie, D. F. Milano, N. A. Deskins, D. Su, X. Teng, *ACS Catal.* **2012**, *2*, 287–297; b) J. Tayal, B. Rawat, S. Basu, *Int. J. Hydrogen Energy* **2012**, *37*, 4597–4605; c) W. Zhou, S. Q. Song, W. Z. Li, Z. H. Zhou, G. Sun, Q. Xin, S. Douvartzides, P. Tsiakaras, *J. Power Sources* **2005**, *140*, 50–58; d) H.-F. Wang, Z.-P. Liu, *J. Am. Chem. Soc.* **2008**, *130*, 10996–11004; e) W. Du, G. Yang, E. Wong, N. A. Deskins, A. I. Frenkel, D. Su, X. Teng, *J. Am. Chem. Soc.* **2014**, *136*, 10862–10865.

[11] A. Kowal, M. Li, M. Shao, K. Sasaki, M. Vukmirovic, J. Zhang, N. Marinkovic, P. Liu, A. Frenkel, R. Adzic, *Nat. Mater.* **2009**, *8*, 325–330.

[12] S. Cha, W. Lee, *J. Electrochem. Soc.* **1999**, *146*, 4055–4060.

[13] R. Loukrakpam, Q. Yuan, V. Petkov, L. Gan, S. Rudi, R. Yang, Y. Huang, S. R. Brankovic, P. Strasser, *Phys. Chem. Chem. Phys.* **2014**, *16*, 18866–18876.

[14] R. Ghosh Chaudhuri, S. Paria, *Chem. Rev.* **2012**, *112*, 2373–2433.

[15] V. D. Colle, M. J. Giz, G. Tremiliosi-Filho, *J. Braz. Chem. Soc.* **2003**, *14*, 601–609.

[16] M. Li, P. Liu, R. R. Adzic, *J. Phys. Chem. Lett.* **2012**, *3*, 3480–3485.

[17] D. Qu, C.-Y. Jung, C.-W. Lee, K. Uosaki, *J. Phys. Chem. C* **2019**, *123*, 2872–2881.

[18] M. J. Hostetler, J. E. Wingate, C.-J. Zhong, J. E. Harris, R. W. Vachet, M. R. Clark, J. D. Londono, S. J. Green, J. J. Stokes, G. D. Wignall, *Langmuir* **1998**, *14*, 17–30.

[19] M. Shao, A. Peles, K. Shoemaker, M. Gummalla, P. N. Njoki, J. Luo, C.-J. Zhong, *J. Phys. Chem. Lett.* **2011**, *2*, 67–72.

[20] M. Shao, A. Peles, K. Shoemaker, *Nano Lett.* **2011**, *11*, 3714–3719.

[21] S. Brankovic, J. Wang, R. Adžić, *Surf. Sci.* **2001**, *474*, L173-L179.

[22] H. Wang, K. Jiang, Q. Chen, Z. Xie, W.-B. Cai, *Chem. Commun.* **2016**, *52*, 374–377.

[23] M. Shao, J. H. Odell, A. Peles, D. Su, *Chem. Commun.* **2014**, *50*, 2173–2176.

[24] L. Gan, C. Cui, S. Rudi, P. Strasser, *Top. Catal.* **2014**, *57*, 236–244.

Manuscript received: March 15, 2020
Revised manuscript received: May 23, 2020
Accepted manuscript online: May 25, 2020
Version of record online: June 12, 2020